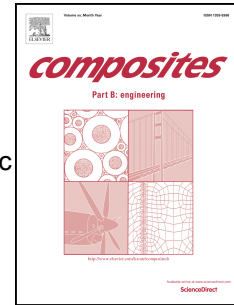


Accepted Manuscript

Assessment of failure toughening mechanisms in continuous glass fiber thermoplastic laminates subjected to cyclic loading

M. Nikforooz, J. Montesano, M. Golzar, M.M. Shokrieh



PII: S1359-8368(18)32449-1

DOI: <https://doi.org/10.1016/j.compositesb.2018.10.065>

Reference: JCOMB 6144

To appear in: *Composites Part B*

Received Date: 3 August 2018

Revised Date: 19 October 2018

Accepted Date: 23 October 2018

Please cite this article as: Nikforooz M, Montesano J, Golzar M, Shokrieh MM, Assessment of failure toughening mechanisms in continuous glass fiber thermoplastic laminates subjected to cyclic loading, *Composites Part B* (2018), doi: <https://doi.org/10.1016/j.compositesb.2018.10.065>.

This is a PDF file of an unedited manuscript that has been accepted for publication. As a service to our customers we are providing this early version of the manuscript. The manuscript will undergo copyediting, typesetting, and review of the resulting proof before it is published in its final form. Please note that during the production process errors may be discovered which could affect the content, and all legal disclaimers that apply to the journal pertain.

Assessment of failure toughening mechanisms in continuous glass fiber thermoplastic laminates subjected to cyclic loadingNikforooz, M^{1,2}, Montesano, J², Golzar, M^{1*}, Shokrieh, MM³,¹ Department of Mechanical Engineering, Tarbiat Modares University, Jalaale-al Ahmad Ave.,
P.O. Box 14115-143, Tehran, Iran² Department of Mechanical & Mechatronics Engineering, University of Waterloo, 200 University Ave.
West, Waterloo, Canada N2L3G1³ Composite Research Laboratory, Center of Excellence in Experimental Solid Mechanics and Dynamics,
School of Mechanical Engineering, Iran University of Science and
Technology (IUST), Narmak, 16846-13114 Tehran, Iran

* Corresponding author (m.golzar@modares.ac.ir; Tel. +98-21-82884320)

Abstract

Tensile fatigue behaviour of glass fiber/polyamide composites, including unidirectional ($[0]_8$, $[90]_8$) and cross-ply ($[0_2/90_2]_s$, $[0_4/90_4]_s$ and $[90_4/0_4]_s$) laminates, was studied and compared to that of similar glass fiber/epoxy composites. The fatigue resistance of cross-ply glass/polyamide was greater than that of glass/epoxy while also exhibiting lower stiffness reduction. To explain this key observation, residual stiffness and residual strength fatigue tests were performed on cross-ply laminates, while optical microscopy was used to measure ply crack density during the different stages of cycling. Testing of the cross-ply laminates at lower peak stresses of 50 % of the ultimate tensile strength (i.e., high cycle fatigue regime) revealed partial cracks that did not propagate completely through the width and thickness of plies due to high matrix toughness and other observed toughening mechanisms such as matrix bridging. A micromechanical finite element model with explicit ply cracks was also used to predict laminate stiffness degradation corresponding to observed ply crack densities, revealing that stiffness degradation was overpredicted when cracks were assumed to span the entire specimen width. Additional finite element simulations with partial cracks showed notably less stiffness reduction. These observations suggest glass/polyamide is inherently more damage tolerant than glass/epoxy and may be a suitable replacement for fatigue critical structures.

Keywords: A. Polymer-matrix composites (PMCs); A. Thermoplastic resin; B. Fatigue; C. Finite element analysis (FEA); D. Mechanical testing; D. Optical microscopy Physical methods of analysis

1. Introduction

Thermoplastic composite materials are gaining much interest in industry owing to numerous advantages they exhibit compared to thermoset composites, including high toughness, good impact resistance and recyclability. However, the fabrication of composite parts using thermoplastic composites remains challenging due to the high viscosity of thermoplastic matrices and associated difficulties in fiber alignment, as well as the higher processing temperatures required to melt thermoplastics. Nevertheless, if these issues can be overcome, fiber-reinforced thermoplastic composites may be a suitable alternative for thermosetting-based composites for some applications.

Thermoplastic composites are candidates for use in structural load-bearing applications, such as wind turbine blades [1] where the structure is exposed to cyclic loading and the fatigue resistance of the material is critical. However, the knowledge on the fatigue behavior of thermoplastic composites is limited to some high-performance thermoplastics such as PEEK and PPS [2,3]. Not only are these thermoplastics expensive, but they also have high melting temperatures which require greater energy and expensive tooling to fabricate large structures such as wind turbine blades. Polyamide is a suitable substitute for the aforementioned thermoplastics, since it is cost-effective and requires much lower energy particularly when it is processed in-situ [1].

A number of studies have utilized particulate polyamide in carbon/epoxy composites to exploit the high toughness of the polyamide matrix for fatigue resistant applications. For example, Takeda et al. [4,5] asserted that the produced toughness-improved composites can arrest transverse cracking and delamination in cross-ply and quasi-isotropic laminates. Ductility and toughness of the matrix may even influence the underlying damage mechanisms more when the matrix is pure polyamide. Therefore, the associated effects should be studied when the designed structure is subjected to fatigue loading.

Recently, glass/polyamide and carbon/polyamide have obtained more interest in industry due to higher stiffness, strength and toughness [6,7], however most of the studies on the fatigue behaviour of

glass/polyamide and carbon/polyamide composites are limited to short fibre composites. Bernasconi et al. [8] and also De Monte et al. [9] investigated the effects of fibre orientation on the fatigue behaviour of short glass fibre/polyamide composites and used the Tsai-Hill criterion to model the fatigue life. Launay et al. [10, 11] attempted to express the constitutive behaviour of short glass fiber/polyamide composites and used dissipated energy as a fatigue index for the estimation of fatigue life. Meneghetti et al. [12] and also Jegou et al. [13] used energy-based failure criteria based on dissipated energy and calibrated the model based on temperature measurements from fatigue tests. Kawai et al. [14] examined the fatigue life of short glass fibre/polyamide composites and used an anisomorphic constant life diagram to predict the fatigue life under different temperatures and stress ratios. They also used micro-computed tomography to study the different modes of failure in the composite.

Studies on the fatigue behaviour of continuous glass/polyamide and carbon/polyamide composites reported in the literature are limited. Cinquin et al. [15] investigated the flexural fatigue behavior of unidirectional glass/polyamide composites in parts of his studies which were limited to displacement control fatigue tests on longitudinal specimens. Rasool [16] characterized the fatigue behavior of woven glass/polyamide and glass/PPS composites experimentally through S-N curves and DIC monitoring of local and global strain fields during cyclic loading and related it to the stiffness degradation of the material. Malpot et al. [17,18] studied the effect of moisture on the static and fatigue behavior of woven glass/polyamide composites and proposed an enhanced model to predict the fatigue life of the composite at any angle and moisture content. They also investigated the influence of moisture on fatigue damage mechanisms through infrared tomography and acoustic emission [19]. Kawai et al. [20] compared the fatigue performance of woven carbon/epoxy and carbon/nylon with and without notches. They observed higher fatigue performance for unnotched carbon/nylon laminates compared to carbon/epoxy laminates. In contrast to the unnotched laminates, the notched carbon/epoxy had higher fatigue performance compared to carbon/nylon. They justified this behavior by more extensive delamination in notched carbon/epoxy laminates compared to carbon/nylon laminates. Ma et al. [21] compared the fatigue

behavior of unidirectional 45° carbon/epoxy and carbon/polyamide composites and examined the residual stiffness and residual strength of the laminates both in low-cycle and high-cycle fatigue region.

It remains clear that there are few studies reported in the literature that assess the fatigue behavior of multidirectional glass/polyamide composites, in particular understanding their distinct damage characteristics. This is important as these materials may be suitable replacements for glass/epoxy composites in structural applications such as wind turbine blades where fatigue resistance is a major concern. For practical applications, laminates with different layups are used to satisfy the stiffness and strength requirements along different directions. Therefore, in order to have a suitable design, the response under cyclic loading should be obtained along different directions for laminates with different lay-ups and compared with those of glass/epoxy.

Therefore, the main objective of this study was to assess the fatigue behaviour of continuous E-glass/polyamide composites at both the lamina and laminate levels and compare the fatigue performance with conventional E-glass/epoxy composites having the same stacking sequences. The fatigue resistance, stiffness and strength degradation, and corresponding damage mechanisms, in different unidirectional and cross-ply glass/polyamide laminates was investigated to improve the understanding of the damage evolution processes under cyclic loading. A micro-mechanical model with explicit cracks assisted in understanding the effects of transverse cracking on stiffness degradation of the cross-ply laminates. To explain further the obtained results for cross-ply laminates, in-situ toughening mechanisms were explored through a detailed damage monitoring approach and their effect on crack evolution was investigated.

2. Materials and experimental set-up

2.1. Process and materials

Unidirectional E-glass/polyamide 6 prepregs from Jonam Composites Ltd. were used to fabricate $[0]_8$, $[90]_8$, $[0_2/90_2]_s$, $[0_4/90_4]_s$ and $[90_4/0_4]_s$ composite laminates via compression moulding using a 30-ton

Carver hot-press and a picture frame mould. A consolidation pressure of 0.9 bar and maximum temperature of 240 °C were used for fabrication of the panels. Further details of the processing parameters, equipment and mould can be found in Ref [22].

2.2. Specimen preparation

Straight-sided and dog bone specimens were cut from 110 mm by 110 mm panels by using a diamond blade saw and water-jet machining, respectively, with geometries and dimensions mentioned in Fig. 1, Table 1 and Table 2. Straight-sided specimens were polished with six different grades of sandpaper and four different grades of alumina powder suspension. Aluminum alloy end tabs were bonded to both ends of the specimen to prevent damage from gripping pressure on the sample.

2.3 Experimental setup

An MTS 810 hydraulic test frame with a 50 kN load cell was used for the testing of $[0]_8$, $[0_4/90_4]_s$ and $[90_4/0_4]_s$ specimens and an Instron 8874 hydraulic test frame with a 25 kN load cell was used for the testing of $[90]_8$ and $[0_2/90_2]_s$ specimens (see Fig. 1). Tension-tension fatigue tests were performed on all laminates until final failure of the specimen. Sinusoidal cyclic loading was applied at the frequency and the load ratio of 10 Hz and 0.1 respectively for different maximum stress levels. Tensile strain was measured using different extensometers on both test frames. Fatigue strength versus the number of cycles to failure ($S-N_f$) and dynamic stiffness versus number of cycles ($E-N$) were extracted.

Furthermore, additional fatigue tests were performed on $[0_2/90_2]_s$ specimens to extract their cyclic damage state and the corresponding residual stiffness. These tests were interrupted at multiple cyclic intervals and quasi-static tensile tests were performed up to the peak strain exhibited during cycling. Digital image correlation (DIC) was employed to measure the strain for these test specimens. Optical microscopes including Olympus BH2-UMA and Olympus Pme3 were used to inspect the polished edge of the specimens and to count the transverse cracks. Furthermore, fractured specimens were cut in the width and length directions and were mounted and polished as previously explained. Both transverse cracks and

longitudinal splitting cracks were inspected in the fractured specimens. Furthermore, scanning electron microscopy was performed on gold coated fracture surfaces using a Phenom-ProX microscope.

In addition to the aforementioned fatigue tests, residual tensile strength at different cyclic loading intervals was measured destructively for a number of specimens with applied peak stress of 50 % of material ultimate tensile strength (UTS). The corresponding quasi-static tensile tests were performed after cyclic loading with a displacement rate of 2 mm/min until specimen failure, in accordance with ASTM D3039.

3. Mechanical test results and discussion

Results of the fatigue tests for all aforementioned glass/polyamide laminates are first presented in this section and compared to similar tests on glass/epoxy laminates from the literature. The interrupted residual stiffness fatigue tests for the $[0_2/90_2]_s$ laminates and residual strength tests for the $[0]_8$ and $[0_n/90_n]_s$ laminates are presented subsequently.

3.1. Tension-tension fatigue tests on $[0]_8$ laminates

S- N_f diagrams with the corresponding fractured specimens for $[0]_8$ glass/polyamide are presented in Fig. 2 and compared with that of glass/epoxy from Ref. [23]. The S- N_f curve for both composites are bi-linear, exhibiting transition knee points at approximately 60 percent of the UTS. Below the knee point (low cycle fatigue region, LCF), the fatigue resistance of glass/polyamide is superior to that of glass/epoxy, however beyond the knee point (high cycle fatigue region, HCF), the two materials manifest approximately the same fatigue resistance. The higher fatigue resistance of glass/polyamide in the LCF region can be circumstantiated by the higher fiber/matrix interfacial toughness of glass/polyamide compared to glass/epoxy, provided by the comparison of the corresponding values in Ref. [24] and Ref. [25] for both material systems with different fiber sizings. In LCF region, the superior glass-polyamide interfacial

toughness resists fiber pull-out so that the mode of failure of glass/polyamide is more step-like, in contrast to brooming which was observed for $[0]_n$ glass/epoxy in Ref. [26].

It is observed that in the LCF region, there are considerably more splitting cracks in the glass/polyamide specimens when compared to the HCF region, and the corresponding failure is quite analogous to the failure in quasi-static loading. In this region, weak fibers as well as misaligned fibers break due to high longitudinal strains. As a consequence of the initial fiber failures, interfacial matrix cracks develop along the fibers provoking interply and intraply splitting cracks (see Fig. 3(a) for 80 and 60 % of the UTS). These cracks are seen in the middle of the specimen. As the peak applied stress decreases, a progressive diminution of the number of splitting cracks and also the length of the cracks will ensue, and at 50 % and 30 % of the UTS some minor cracks can be observed, primarily near the specimen free edges. As seen in Fig. 3(b), for the 50% of the UTS, longitudinal cracks advance partially through the length of the specimens, which shows that ductile behavior of the polyamide matrix prevails at this stress level.

Plots of normalized E-N diagrams with corresponding width-wise sections of fractured samples for some stress levels are shown in Fig. 3. As the maximum stress level increases, the splitting cracks and therefore stiffness degradation increases, however, glass/polyamide laminates experience lower stiffness reduction in their fatigue lifetime compared to glass/epoxy [27]. The stiffness degradation is negligible for the two materials prior to final failure, where sudden degradation occurs just before specimen failure ensues.

To provide further support for the fatigue resistance comparison between glass/polyamide and glass/epoxy in HCF region, the residual strength after fatigue of $[0]_8$ glass/polyamide was obtained experimentally at 50 % of the UTS and compared with that of $[0]_n$ glass/epoxy from Ref. [28]. As shown in Fig. 4. Equation (1) from Ref. [29] was used to normalize the data so that the data is independent of stress ratio, stress level and number of cycles to failure.

$$\left[\frac{R-\sigma}{R_s-\sigma} \right] = \left[1 - \left[\frac{\log(n)-\log(0.25)}{\log(N_f)-\log(0.25)} \right]^\alpha \right]^\beta \quad (1)$$

Here, σ is the maximum applied fatigue stress, n is number of cycles, N_f is number of cycles to failure, R_s is quasi-static tensile strength. α and β are empirical coefficients.

As indicated in Fig. 4, the residual strength after fatigue of $[0]_8$ glass/polyamide is comparable to that of glass/epoxy. This result further corroborates the fatigue resistance comparison performed in Fig. 2 for $[0]_n$ glass/polyamide and glass/epoxy at 50 % the UTS.

3.2. Tension-tension fatigue tests on $[90]_8$ laminates

Plots of $S-N_f$ and the normalized E-N diagrams for $[90]_8$ glass/polyamide and glass/epoxy composites from Ref. [23] are shown in Fig. 5. Basquin's power-law equation was utilized for fitting of the experimental data as indicated in equation (2). Conversely to $[0]_n$, the fatigue resistance of $[90]_8$ glass/epoxy is greater than that of glass/polyamide. This result is reasonable since the transverse quasi-static strength of glass/epoxy is more than 2.5 times higher than that of glass/polyamide [22].

$$S = A(N_f)^B \quad (2)$$

However, fatigue sensitivity is higher in glass/epoxy compared to glass/polyamide which possesses lower Basquin's slope and experiences less stiffness degradation during its fatigue lifetime. This observation can be explained by the superior interlaminar fracture toughness [30] augmented by some predominant toughening mechanisms such as fiber and ligament bridging observed in $[90]_8$ glass/polyamide during crack wake opening (see Fig. 6). It is mentioned that fiber bridging is well known in thermoset composites which have comparatively low fiber/matrix interfacial strength [31], leading to debonding and slipping of the fibers relative to the matrix. The left intact fibers will subsequently break by further opening of the crack wake. However ligament bridging is primarily associated with the high ductility of the polyamide matrix in $[90]_8$ glass/polyamide laminate. In other words, cracks start growing from the fiber/matrix interface and after reaching the ductile polyamide matrix, they are arrested. At the same time cracks nucleate from an adjacent fracture plane leaving a bridging ligament in the crack wake. Ligament

bridging restrains the crack opening displacements, contributing to lower crack progression. In this way $[90]_8$ glass/polyamide fails more in a sudden manner compared to $[90]_n$ glass/epoxy.

3.3. Tension-tension fatigue tests on $[0_n/90_n]_s$ and $[90_n/0_n]_s$ Laminates

Plots of $S-N_f$ and the normalized E-N diagrams of $[0_2/90_2]_s$, $[0_4/90_4]_s$ and $[90_4/0_4]_s$ glass/polyamide and $[0_2/90_2]_s$ glass/epoxy laminates [32,33] are presented in Fig. 7(a-c) and Fig. 7(d), respectively. It can be observed that all the $[0_n/90_n]_s$ glass/polyamide laminates exhibit the same Basquin's slope though higher intercept compared to $[0_2/90_2]_s$ glass/epoxy laminates. This result is noticeable, since it indicates that the fatigue lifetime of $[0_n/90_n]_s$ glass/polyamide is longer than that of glass/epoxy for any applied peak stress level and for different ply thicknesses. Furthermore, the dynamic stiffness degradation of different laminations of glass/polyamide is lower than that of $[0_2/90_2]_s$ glass/epoxy.

It is also known from Ref. [22] that transverse cracking initiation strain and also the quasi-static strength of $[0_2/90_2]_s$ glass/polyamide are higher compared to similar glass/epoxy laminates. Treating longitudinal and transverse layers as the critical and non-critical elements (i.e. the $[0]_n$ layers as load bearing elements and $[90]_n$ as stiffness determining elements) can explain this key observation. In other words, superior fatigue strength of $[0]_n$ laminates and low stiffness degradation of $[0]_n$ and $[90]_n$ laminates compared to glass/epoxy justify the observed fatigue behavior of $[0_2/90_2]_s$ laminates compared to glass/epoxy to some extent; however, deep investigation of the fatigue behaviour of $[0_n/90_n]_s$ glass/polyamide will be presented in section 3.4 and 3.5.

As depicted in Fig. 7(b), the fatigue resistance of $[0_2/90_2]_s$ laminate is higher than that of $[0_4/90_4]_s$ laminate. It is well known that the free edges of $[0_n/90_n]_s$ laminates exhibit a 3-D stress field in simple tension due to the existence of interlaminar stresses. The distance from the free edges in which these stresses exist is approximately twice the ply thickness [34]. As the ply thickness increases, the magnitude of the normal interlaminar stresses and the volume in which these stresses are effective increase [35]. This raises the likelihood of delamination at lower stress levels [36] near the specimen free edges contributing

to the lower fatigue life of the $[0_4/90_4]_s$ laminates. Furthermore, this reduction in fatigue life is supported by Ref. [37] and low magnification optical microscopy in fatigue loading in Fig. 8, where more splitting cracks were observed in $[0_4/90_4]_s$ glass/polyamide laminates compared to $[0_2/90_2]_s$ laminates. As seen in Fig. 9(a), the trend of stiffness degradation of $[0_4/90_4]_s$ laminate is identical to that of the $[0_2/90_2]_s$ laminate despite having double thickness. However, the total stiffness degradation of $[0_4/90_4]_s$ is lower which can be explained by its lower life compared to $[0_2/90_2]_s$ laminate and the reduced time for crack multiplication.

As demonstrated in Fig. 7(c), the fatigue resistance of $[90_4/0_4]_s$ laminates is higher than that of $[0_4/90_4]_s$ laminates, which has also been observed for glass/phenolic in Ref. [38]. This result is explained by the comparison of stiffness degradation and cracking of the two laminates in Fig. 9(b). The transverse crack density at saturation level is lower in $[90_n/0_n]_s$ compared to $[0_n/90_n]_s$ laminates [39] due to the reduced constraining effect on transverse plies in $[90_n/0_n]_s$ laminates. The measured crack density was $0.4 \text{ (mm}^{-1}\text{)}$ in $[90_4/0_4]_s$ compared to $0.545 \text{ (mm}^{-1}\text{)}$ from Ref. [37]. Consequently, $[90_4/0_4]_s$ has less initial stiffness degradation as a result of reduced transverse matrix cracking. Comparison of $[0_n/90_n]_s$ and $[90_n/0_n]_s$ laminates in Ref. [35] has shown that the magnitude of through the thickness stress, σ_z is lower in $[90_n/0_n]_s$ than $[0_n/90_n]_s$ laminates, furthermore, the nature of σ_z in $[90_n/0_n]_s$ laminates is negative in contrast to positive nature of σ_z in $[0_n/90_n]_s$ laminates. This prevents potential splitting cracks and local delamination to develop after saturation of transverse cracks which also justifies the lower stiffness degradation after saturation of transverse cracks. SEM observations of the fracture surfaces in $[90_n/0_n]_s$ show low splitting cracks and some local plastic deformation in polyamide matrix in 0° and 90° layers. This plastic deformation prevents splitting cracks to develop in 0° layers and the final fracture is brittle with local fiber fractures in $[90_n/0_n]_s$ laminates (see Fig. 10). These results can corroborates the slightly higher fatigue life of $[90_n/0_n]_s$ compared to $[0_n/90_n]_s$ laminates.

3.4. Damage characterization and residual stiffness degradation in $[0_2/90_2]_s$ laminates

Residual stiffness degradation and transverse crack density versus number of cycles for $[0_2/90_2]_s$ laminates were measured at different maximum stress levels of 50 %, 60 %, 70 % and 80 % of the UTS, and are presented herein. Cross-ply glass/polyamide composites exhibited three stages of damage evolution depending on the maximum applied stress levels. Stage I manifests as transverse cracking and causes the largest stiffness degradation over the fatigue lifetime, stage II is characterized by delamination and splitting and causes less stiffness degradation compared to stage I, and stage III is fiber failure and causes great stiffness degradation prior to the final failure of the composite laminate.

3.4.1. Transverse cracking and toughening mechanisms

For all stress levels, transverse micro-cracks with different lengths initiated early in the cycling of the laminates. The cracks originated from the free edges at the fiber-matrix interface due to the associated stress concentration. Some of the cracks grew quite rapidly through the thickness at the beginning, however as the crack density increased, the growth rate decreased noticeably. This observation is in contrast to the transverse cracking in some other thermoplastic material systems, where transverse cracking initiates late in the fatigue lifetime and reaches the saturation level very fast [40,41]. Fig. 11 presents the progression of two representative cracks in the thickness direction of a $[0_2/90_2]_s$ laminate at 50 % of the UTS. Crack A propagates completely after 50 cycles but it takes nearly most of the lifetime for crack B to propagate due to the exposed crack tip shielding caused by crack A. This effect contributes to the tip plasticization of crack B. The behavior is rarely observed in thermoset composites in which nearly all of the transverse cracks span across the thickness instantly [42].

Only complete transverse cracks were counted at different number of cycles as indicated by Fig. 12 until the crack density reached the saturation level. As the stress level increased, the crack multiplication rate increased proportionally. As represented in Fig. 12(b), the crack density at saturation level is approximately the same for all stress levels and is comparable to the crack density at saturation for quasi-

static loading. This result affirms that crack density is a laminate property for thermoplastic glass/polyamide as it depends on the material and laminate stacking sequence, as has been mentioned for other thermoset material systems [43].

In contrast to the propagation of crack A and crack B in Fig. 11, some of the cracks develop non-uniformly along the fiber-matrix interfaces. In other words, these cracks reach the resin rich areas or the misaligned fibers and either change their propagation path if they find surrounding fiber-matrix interfaces (Fig. 13(a)) or they are arrested. In the former situation, tortuous crack fronts are created and in the latter case four different scenarios may occur. First, cracks are suppressed and do not propagate until the final failure of the laminate. This can be explained by crack blunting at the tip of the cracks, which is intensified by the crack tip shielding caused by adjacent cracks (Fig. 13(b)). Second, cracks bridge the tough polyamide matrix and nucleate from the neighbor of the existing resin rich area (Fig. 13 (c)). Sometimes the resin rich area is so vast that the new crack nucleate far from the existing crack (Fig. 13(d)). Matrix bridging can occur repeatedly during the complete growth of a transverse crack, however these intermittent cracks cannot coalesce into one dominant crack. In another situation, cracks propagate from a different fracture plane in the opposite direction. These two cracks cannot merge and there is a gap between them recalling ligament bridging which was observed in fatigue failure of 90° composite laminates (see Fig. 13(e) and Fig. 6). In the final situation, when the transverse crack reaches the not well-distributed fibers or tough polyamide matrix, it branches into smaller micro-cracks which is called bifurcation (Fig. 13(f) and Fig. 13(g)). These toughening mechanisms deflect the crack wakes and cause meandering and jagged crack surfaces, therefore contribute to more energy dissipation through increasing total fracture area.

A micromechanical model developed in [44] was employed to model the stiffness degradation in glass/polyamide composites. Ansys APDL was used to model the representative volume element (RVE) of half the symmetric laminate with one crack in the 90° ply. Twenty-node brick elements were exerted

for finite element meshing of the laminate, as seen in Fig. 14. The plies were assumed to have transversely orthotropic homogenized properties, while periodic boundary conditions were applied.

It is noteworthy that the micromechanical model only simulates the stiffness degradation arising from transverse cracking and does not account for stiffness degradation caused by splitting cracks, delamination and fiber failure. Measured transverse crack density is utilized as an input for the model. The model assumes that the transverse cracks propagate through the entire width of the specimen instantaneously after they are initiated from the specimen free edges. As represented in Fig. 15, the stiffness predicted by the model at 60 %, 70 % and 80 % of the UTS coincides well with the measured stiffness until crack density approaches the saturation level. However, the model overestimates the stiffness degradation at 50 % of the UTS. The difference presumably is attributed to the transverse cracks that propagate partially through the width and thickness of the specimen at this stress level in opposition to the assumption made by the model. Another reason for this difference is the higher probability of non-existence of dominant cracks at 50 % of the UTS in the case of crack bridging as was indicated in Fig. 13.

To ascertain the existence of partial width-wise cracks, the fatigue test was conducted on two $[0_2/90_2]_s$ specimens at 50 % of the UTS. One of specimens was stopped after 140 cycles and the other sample was stopped at 4000 cycles corresponding to the early stage of micro-cracking and post saturation at this stress level, respectively. The two specimens were cut in the middle along the fiber direction to inspect the transverse crack density. For the first sample which was stopped at 140 cycles, the crack density was $1.24(\text{mm}^{-1})$ in the edge however, it was $0.96(\text{mm}^{-1})$ in the middle of the specimen. It is mentioned that the partial thickness-wise cracks were comparable in the edge and in the middle of the specimen. This observation confirms that the cracks cannot smear completely through the width of the specimens at early stage of cycling.

For the other test which was stopped after 4000 cycles, the crack densities were nearly the same in the edge and in the middle of the specimen. Considering that the transverse crack density saturates after 2000 cycles, this observation confirms that the second hypothesis is true and the lack of dominant transverse

cracks due to the aforementioned toughening mechanisms at 50 % of the UTS causes the stiffness difference between the experiments and the finite element model.

The effects of partial width-wise ply cracks on stiffness degradation was investigated by invoking the model in Ref. [44]. The model was modified to consider partial cracks with different lengths in conjunction with these assumptions: the crack length increases gradually with number of cycles as in Ref. [45] and there is an average crack length at a specified number of cycle. The model was run for different crack lengths and two different crack densities. As illustrated in Fig. 16(a) as the length of the cracks reaches its total length, the rate of the stiffness degradation increases. This result again corroborates the large difference observed between the stiffness degradation predicted by the model and the experiment at early stage of cycling in 50 % of the UTS.

3.4.2. Splitting cracks and delamination

As seen in Fig. 15, the main mechanism in the second stage of stiffness degradation is splitting for different maximum stress levels, while splitting was observed at a much lower extent for 50 % of the UTS, which is consistent with the results for splitting of $[0]_8$ laminates (see Fig. 3(b)). As indicated in Fig. 3(b) and Fig. 15(a), the extent of splitting is noticeably low at medium to low stress levels, therefore the external energy cannot be dissipated in the form of splitting to reduce the stress concentration at the interface between longitudinal and transverse layers. In this condition due to the lack of splitting cracks and delamination, stress concentration at the tip of the transverse cracks causes local fiber failures which are reflected as sudden falls in the stiffness versus number of cycles diagram (see Fig. 15(a)).

Delamination was exclusively observed in two specimens among the eleven tested specimens (see Fig. 15(c) for 70 % of the UTS). This can be justified by the high interlaminar fracture toughness of the laminate [30] which increased the plastic zone size at the tip of the transverse cracks and relieved the corresponding stress concentration hereby mitigated delamination. Instead of delamination, splitting cracks were observed predominantly at the specimen edges in 0° layer. When delamination initiated

between longitudinal and transverse layers it contributed to dissipate the energy and decreased the number of splitting cracks noticeably. In the case of thermoplastic glass/polyamide, delamination is intermittent, therefore at the tip of transverse cracks and delamination front, numerous number of longitudinal fibers broke locally due to the associated stress concentration (see Fig. 15(c)) and caused the final failure of the laminate. For 80 % of the UTS, large splitting cracks instantly caused fiber failure. As seen in Fig. 15(d), there are residues of longitudinal layer on transverse layer which confirms the high resistance of polyamide matrix to delamination.

3.5. Residual strength of $[0_n/90_n]_s$ glass/polyamide laminates after cyclic loading

The effect of transverse cracks was investigated on the residual strength of the cross-ply laminates. For this purpose, the residual strength after fatigue of $[0_2/90_2]_s$ and $[0_4/90_4]_s$ glass/polyamide at 50 % of the UTS was obtained experimentally and was normalized using equation (1). As seen in Fig. 17, the residual fatigue strength of $[0]_8$, $[0_2/90_2]_s$ and $[0_4/90_4]_s$ laminates exhibits a large scatter in stage I and stage III, however the scatter is much lower in stage II. The observed scatter arises from two sources of damage i.e. stage I correlates to the initiation of transverse micro-cracking and stage III is close to the final failure of the material. In stage II, damage accumulates at a lower rate, therefore the residual strength data converges noticeably.

In stage I of cycling, it appears that the transverse micro-cracking does not affect the residual fatigue strength, since the residual strength data are in the same scatter band. In stage II as explained in the previous section, delamination is impeded by the high toughness of the polyamide matrix, however minor splitting cracks and local fibre failure at the tip of the transverse cracks during the fatigue loading affect the residual fatigue strength to a great extent (see Fig. 15(a)). As seen in Fig. 17, the normalized residual strength changes from 0.64 to 0.76 for $[0_2/90_2]_s$ laminates, however it changes from 0.76 to 0.88 for $[0]_8$ laminates.

Furthermore, the residual strength of $[0_4/90_4]_s$ was compared to that of $[0]_8$ laminates. It was found that the residual strength of $[0_4/90_4]_s$ is more similar to $[0]_8$ laminates compared to $[0_2/90_2]_s$ laminates. There are two reasons for this observation. Firstly, the number of 0° layers in $[0_4/90_4]_s$ is the same as in $[0]_8$ laminate. Secondly, as shown in Ref. [37], transverse crack density at the saturation level is much lower in $[0_4/90_4]_s$ compared to $[0_2/90_2]_s$ laminates thus there is a lower probability of local fibre failure at the tip of the transverse cracks. However, there are more and larger splitting cracks in $[0_4/90_4]_s$ compared to $[0_2/90_2]_s$ laminates [37]. This observation suggests that as the ply thickness increases in $[0_n/90_n]_s$ laminates, the behaviour of the laminate is more affected by longitudinal cracks than transverse cracks. These findings contradict what was mentioned in the comparison of the fatigue behaviour of carbon/epoxy and carbon/PEEK in Ref. [46], mentioning that the transverse cracks do not contribute to the fatigue behaviour of cross-ply thermoplastic carbon/PEEK laminates.

As it was shown in Fig. 3(a) and Fig. 15, as the stress level increases the number of splitting cracks increases. It is anticipated that as the stress level and number of layers increases in $[0_n/90_n]_s$ i.e. 60 %, 70 % and 80 % of the UTS, the residual strength of the laminates is less affected by the transverse cracks, since splitting cracks and possible delamination at the laminate free edges dissipate the energy and help to redistribute the stress field at the free edges and therefore prevent the local build-up of the fiber fractures.

4. Conclusions

Fatigue behaviour of glass/polyamide composites, including unidirectional ($[0]_8$, $[90]_8$) and cross-ply ($[0_2/90_2]_s$, $[0_4/90_4]_s$ and $[90_4/0_4]_s$) laminates, was investigated through an experimental test program and compared with that of glass/epoxy from the literature. The inherent microscopic toughening mechanisms of the glass/polyamide cross-ply laminates directly influencing their fatigue performance were identified, and the resulting fatigue resistance was notably enhanced compared to that of glass/epoxy laminates. The main conclusions are summarized as follows:

- Fatigue tests on $[0]_n$ and $[90]_n$ glass/polyamide specimens revealed local toughening mechanisms, including local plastic deformation of the polyamide matrix and fiber/ligament bridging, which restricted or arrested the propagation of microcracks. As a result, the glass/polyamide test specimens exhibited little stiffness degradation and low fatigue sensitivity.
- Fatigue tests on the glass/polyamide cross-ply laminates revealed additional toughening mechanisms, such as crack tip blunting, matrix bridging and crack branching, which resulted in lower stiffness degradation and increased fatigue resistance when compared to similar glass/epoxy cross-ply laminates from the literature. As a result of local toughening effects, partial width-wise 90° ply cracks and localized 0° ply splitting cracks were observed in glass/polyamide specimens loaded in the high cycle fatigue regime, resulting in lower stiffness degradation which was confirmed by micromechanical finite element predictions. Specimens cycled in the low cycle fatigue regime exhibited full width-wise 90° ply cracks and larger and more extensive 0° ply splitting cracks.
- Comparison of different glass/polyamide cross-ply laminates revealed lower fatigue resistance for $[0_n/90_n]_s$ laminates compared to $[90_n/0_n]_s$ laminates. The nature of through-thickness normal stresses at the $[90_n/0_n]_s$ specimen free edges resulted in fewer 0° ply splitting cracks and therefore longer fatigue lives. Microscopic observations of fracture surfaces also revealed more extensive local matrix plastic deformation in $[90_n/0_n]_s$ laminates.
- The inherent relation between 90° ply transverse cracking and residual tensile strength after cyclic loading of cross-ply laminates was postulated depending on the ply thickness. In $[0_2/90_2]_s$ laminates, transverse cracks were observed to not influence the residual strength during the early stage of damage development; however, during the latter stages of cycling transverse cracks affected the residual strength due to the localized fiber failure at the tip of the saturated transverse cracks. In $[0_4/90_4]_s$ laminates the residual strength was less affected by transverse cracking since 0° ply splitting cracks were more dominant.

The rigorous assessment of a continuous glass fiber-reinforced polyamide thermoplastic composite material presented is decisive and robust, and fills a current gap in the literature. The study is considered to be a significant step towards using glass/polyamide laminates for fatigue critical structures such as wind turbine blades.

Acknowledgements

Tarbiat Modares University and the University of Waterloo are greatly acknowledged for financial support of this study. The members of the Fatigue and Stress Analysis Laboratory at the University of Waterloo are also acknowledged for their support in conducting all the fatigue experiments.

References

- [1] Rijswijk KV, Thermoplastic composite wind turbine blades, Ph.D. thesis, Delft University of Technology, Delft, 2006.
- [2] Spearing SM, Beaumont PWR, Kortschot MT. The fatigue damage mechanics of notched carbon fibre/PEEK laminates. *Composites* 1992;23:305–11.
- [3] Vieille B, Albouy W, Bouscarrat D, Taleb L. High-temperature fatigue behaviour of notched quasi-isotropic thermoplastic and thermoset laminates: Influence of matrix ductility on damage mechanisms and stress distribution. *Compos Struct* 2016;153:311–20.
- [4] Takeda N, Ogihara S, Kobayashi A, Song DY. Microscopic fatigue failure process in interleaved and toughness-improved CFRP cross-ply laminates. *Adv Compos Mater* 1997.
- [5] Takeda N, Kobayashi S, Ogihara S, Kobayashi A. Effects of toughened interlaminar layers on fatigue damage progress in quasi-isotropic CFRP laminates. *Int J Fatigue* 1999.
- [6] van Dijk YLM, Grätzl T, Abouhamzeh M, Kroll L, Shroff S. Hygrothermal viscoelastic material characterisation of unidirectional continuous carbon-fibre reinforced polyamide 6. *Compos Part B Eng* 2018;150:157–64.
- [7] Spronk SWF, Kersemans M, De Baerdemaeker JCA, Gilibert FA, Sevenois RDB, Garoz D, et al. Comparing damage from low-velocity impact and quasi-static indentation in automotive carbon/epoxy and glass/polyamide-6 laminates. *Polym Test* 2018;65:231–41.
- [8] Bernasconi A, Davoli P, Basile A, Filippi A. Effect of fibre orientation on the fatigue behaviour of a short glass fibre reinforced polyamide-6. *Int J Fatigue* 2007;29:199–208.
- [9] De Monte M, Moosbrugger E, Quaresimin M. Influence of temperature and thickness on the off-axis behaviour of short glass fibre reinforced polyamide 6.6 - Cyclic loading. *Compos Part A Appl Sci Manuf* 2010;41:1368–79.
- [10] Launay A, Maitournam MH, Marco Y, Raoult I, Szmytka F. Cyclic behaviour of short glass fibre reinforced polyamide: Experimental study and constitutive equations. *Int J Plast* 2011;27:1267–93.
- [11] Launay A, Maitournam MH, Marco Y, Raoult I. Multiaxial fatigue models for short glass fibre reinforced polyamide. Part II: Fatigue life estimation. *Int J Fatigue* 2013;47:390–406.
- [12] Meneghetti G, Quaresimin M. Fatigue strength assessment of a short fiber composite based on the specific heat dissipation. *Compos Part B* 2011;42:217–25.
- [13] Jegou L, Marco Y, Saux V Le, Calloch S. Fast prediction of the Wöhler curve from heat build-up measurements on Short Fiber Reinforced Plastic. *Int J Fatigue* 2013;47:259–67.
- [14] Kawai M, Takeuchi H, Taketa I, Tsuchiya A. Composites : Part A Effects of temperature and stress ratio on fatigue life of injection molded short carbon fiber-reinforced polyamide composite. *Compos Part A* 2017;98:9–24.

- [15] Cinquin J, Chabert B, Chauchard J, Morel E, Trotignon JP. Characterization of a thermoplastic (polyamide 66) reinforced with unidirectional glass fibres. Matrix additives and fibres surface treatment influence on the mechanical and viscoelastic properties. *Composites* 1990;21:141–7.
- [16] Rasool S, Fatigue of woven thermoplastic composites: the effect of fiber matrix interface, Ph. D. thesis, Department of mechanical engineering, Delft University of Technology, Delft, 2015.
- [17] Malpot A, Touchard F, Bergamo S. Influence of moisture on the fatigue behaviour of a woven thermoplastic composite used for automotive application. *Mater Des* 2016;98:12–9.
- [18] Malpot A, Touchard F, Bergamo S. Fatigue Behaviour of a Thermoplastic Composite Reinforced with Woven Glass Fibres for Automotive Application. *Procedia Eng* 2015;133:136–47.
- [19] Malpot A, Touchard F, Bergamo S. An investigation of the influence of moisture on fatigue damage mechanisms in a woven glass-fibre-reinforced PA66 composite using acoustic emission and infrared thermography. *Compos Part B Eng* 2017;130:11–20.
- [20] Kawai M, Morishita M, Fuzi K, Sakurai T, Kemmochi K. Effects of matrix ductility and progressive damage on fatigue strengths of unnotched and notched carbon fibre plain woven roving fabric laminates. *Compos Part A Appl Sci Manuf* 1996;27:493–502.
- [21] Ma Y, Zhang Y, Sugahara T, Jin S, Yang Y, Hamada H. Off-axis tensile fatigue assessment based on residual strength for the unidirectional 45° carbon fiber-reinforced composite at room temperature. *Compos Part A Appl Sci Manuf* 2016;90:711–23.
- [22] Nikforooz M, Golzar M, Shokrieh MM, Montesano J. Processability and tensile performance of continuous glass fiber/polyamide laminates for structural load-bearing applications. *Compos Part A Appl Sci Manuf* 2018;105:156–64.
- [23] <https://www.wmc.eu/optimatbladesdocs.php>.
- [24] Pegoretti A, Accorsi ML, Dibenedetto AT. Fracture toughness of the fibre-matrix interface in glass-epoxy composites. *J Mater Sci* 1996;31:6145–53.
- [25] Pegoretti A, Fidanza M, Migliaresi C, Dibenedetto AT. Toughness of the fiber / matrix interface in nylon-6 / glass fiber composites. *Compos Part A Appl Sci Manuf* 1997:283–91.
- [26] Harik VM, Klinger JR, Bogetti TA. Low-cycle fatigue of unidirectional composites: Bi-linear S-N curves. *Int J Fatigue* 2002;24:455–62.
- [27] Eliopoulos EN, Philippidis TP. A progressive damage simulation algorithm for GFRP composites under cyclic loading. Part I: Material constitutive model. *Compos Sci Technol* 2011;71:742–9.
- [28] Philippidis TP, Passipoularidis VA. Residual strength after fatigue in composites: Theory vs. experiment. *Int J Fat* 2007;29:2104-2116.
- [29] Shokrieh MM, Lessard LB. Progressive fatigue damage modeling of composite materials, part I: Modeling. *J Compos Mater* 2000;34:1056–80.
- [30] Chen JH, Schulz E, Bohse J, Hinrichsen G. Effect of fibre content on the interlaminar fracture toughness of unidirectional glass-fibre/polyamide composite. *Compos Part A Appl Sci Manuf* 1999;30:747–55.
- [31] Feih S, Wei J, Kingshott P, Sørensen BF. The influence of fibre sizing on the strength and fracture toughness of glass fibre composites. *Compos Part A Appl Sci Manuf* 2005;36:245–55.
- [32] Roundi W, El Mahi A, El Gharad A, Rebière J-L. Experimental and numerical investigation of the effects of stacking sequence and stress ratio on fatigue damage of glass/epoxy composites. *Compos Part B Eng* 2016;109.
- [33] Shen H, Yao W, Qi W, Zong J. Experimental investigation on damage evolution in cross-ply laminates subjected to quasi-static and fatigue loading. *Compos Part B Eng* 2017;120:10–26.
- [34] Chung S, Effects of Interlaminar Stress Gradients on Free Edge Delamination in Composite Laminates, Ph.D. thesis, Drexel University, Philadelphia, 2003.
- [35] Lessard LB, Schmidt AS, Shokrieh MM. Three-dimensional stress analysis of free-edge effects in a simple composite cross-ply laminate. *Int J Solids Struct* 1996;33:2243–59.
- [36] Lagunegrand L, Lorriot T, Harry R, Wargnier H, Quenisset JM. Initiation of free-edge delamination in composite laminates. *Compos Sci Technol* 2006;66:1315–27.

- [37] Nikforooz M, Montesano J, Golzar M, Shokrieh MM. Assessment of the thermomechanical performance of continuous glass fiber-reinforced thermoplastic laminates. *Polym Test* 2018;67:457–67.
- [38] Moura Branco C, Ferreira JM, Fael P, Richardson MOW. A comparative study of the fatigue behaviour of GRP hand lay-up and pultruded phenolic composites. *Int J Fatigue* 1996;18:255–63.
- [39] Smith PA, Boniface L, Glass NFC. A Comparison of Transverse Cracking Phenomena in (0/90)_s and (90/0)_s CFRP Laminates. *Appl Compos Mater* 1998;5:11–23.
- [40] Diao X, Ye L, Mai Y. Fatigue behaviour of CF/PEEK composite laminates made from commingled prepreg. Part I: experimental studies. *Compos Part A Appl Sci Manuf* 1997;28:739–47.
- [41] Henaffgardin C, Lafariefrenot MC. Fatigue behavior of thermoset and thermoplastic cross-ply laminates. *Composites* 1992;23:109:116.
- [42] Boniface L, Ogini SL. Application of the Paris Equation to the Fatigue Growth of Transverse Ply Cracks. *J Compos Mater* 1989.
- [43] Reifsnider KL, Talug A. Analysis of fatigue damage in composite laminates. *Int J Fatigue* 1980;2:3–11.
- [44] Montesano J, Singh CV. A synergistic damage mechanics based multiscale model for composite laminates subjected to multiaxial strains. *Mech Mater* 2015;83:72–89.
- [45] Berthelot JM, El Mahi A, Leblond P. Transverse cracking of cross-ply laminates: Part 2. Progressive widthwise cracking. *Compos Part A Appl Sci Manuf* 1996;27:1003–10.
- [46] Dickson, R.F., C.J. Jones, B. Harris, D.C. Leach and DRM. The Environmental Fatigue Behaviour of Carbon Fibre Reinforced Polyether Ether Ketone. *J Mater Sci* 1985;20:60–70.

Figures

Fig. 1. a) MTS 810 fatigue testing frame and b) Instron 8874 fatigue testing frame and c) geometry of the straight-sided and dog bone specimens used for fatigue tests.

Fig. 2. S-N diagram of [0]_n glass/epoxy [23] and [0]₈ glass/polyamide composites with the corresponding fractured specimens.

Fig. 3. a) Width-wise cross-section of fractured [0]₈ glass/polyamide under cyclic loading at different stress levels. b) Partial splitting crack in a representative [0]₈ specimen fatigued at 50 % of the UTS. c) Comparison of normalized dynamic stiffness versus normalized number of cycles for [0]_n glass/polyamide and glass/epoxy laminates.

Fig.4. Normalized residual strength versus normalized number of cycles for [0]_n glass/epoxy and [0]_n glass/polyamide laminates cycled at 50 % of the UTS.

Fig. 5. a) Maximum stress versus number of cycles to failure and b) Dynamic stiffness versus the number of cycles for [90]_n glass/polyamide and [90]_n glass/epoxy.

Fig.6. a) Optical image and b) SEM micrographs of ligament bridging at the crack wake of [90]_n glass/polyamide laminates after fatigue failure.

Fig. 7. Comparison of S-N diagrams between a) [0₂/90₂]_s glass/PA and [0₂/90₂]_s glass/epoxy, b) [0₂/90₂]_s glass/PA and [0₄/90₄]_s glass/PA, c) [0₄/90₄]_s glass/PA and [90₄/0₄]_s glass/PA d) Normalized dynamic stiffness versus normalized number of cycles for [0₂/90₂]_s, [0₄/90₄]_s, [90₄/0₄]_s glass/polyamide and [0₂/90₂]_s glass/epoxy laminates.

Fig. 8. Post-mortem optical images of the fracture surfaces in a) [0₂/90₂]_s and b) [0₄/90₄]_s glass/polyamide laminates after fatigue loading.

Fig. 9. Diagram of normalized dynamic stiffness versus the number of cycles for a) [0₂/90₂]_s and [0₄/90₄]_s laminates for 50 % and 60 % of the UTS, b) [0₄/90₄]_s and [90₄/0₄]_s laminates for 50 % and 60 % of the UTS.

Fig. 10. SEM micrographs of the fracture surfaces in a) $[0_2/90_2]_s$ and b) $[90_4/0_4]_s$ laminates after fatigue loading.

Fig. 11. Growth of two representative transverse cracks through the thickness of the 90° layer in a $[0_2/90_2]_s$ laminate for different number of cycles at 50 % of the UTS.

Fig. 12. a) Crack density versus the number of applied cycles for $[0_2/90_2]_s$ laminates at different maximum stress levels and b) Comparison of the saturated crack density for multiple $[0_2/90_2]_s$ laminates under fatigue at different maximum stress levels and quasi-static loading.

Fig. 13. Different toughening mechanisms in transverse cracking of 90° layer in $[0_2/90_2]_s$ laminates at 50 % of the UTS (yellow arrows indicate the resin rich areas).

Fig. 14. Schematic representation of the half of the $[0_n/90_n]_s$ laminate used in FEM modeling.

Fig. 15. Residual stiffness versus the number of cycles and the underlying damage modes in $[0_2/90_2]_s$ glass/polyamide for different maximum stress levels of a) 50 % the UTS b) 60 % the UTS c) 70 % the UTS d) 80 % the UTS.

Fig. 16. a) Normalized residual stiffness versus crack length for two different transverse crack densities b) Schematic of transverse crack propagation in $[0_n/90_n]_s$ laminates.

Fig.17. Normalized residual strength versus the normalized number of cycles for $[0]_8$, $[0_2/90_2]_s$, $[0_4/90_4]_s$ laminates.

Tables

Table 1. Dimensions of the straight-sided specimens used for fatigue tests.

Laminations	L_1 (mm)	L_2 (mm)	H_1 (mm)	H_2 (mm)	W_1 (mm)
$[0]_8$, $[0_2/90_2]_s$	110	20	10	1.4 ± 0.1	15 ± 0.1
$[0_4/90_4]_s$, $[90_4/0_4]_s$	110	20	10	2.8 ± 0.1	15 ± 0.1
$[90]_8$	110	20	10	1.4 ± 0.1	20 ± 0.1

Table 2. Dimensions of the dog-bone specimens used for fatigue tests.

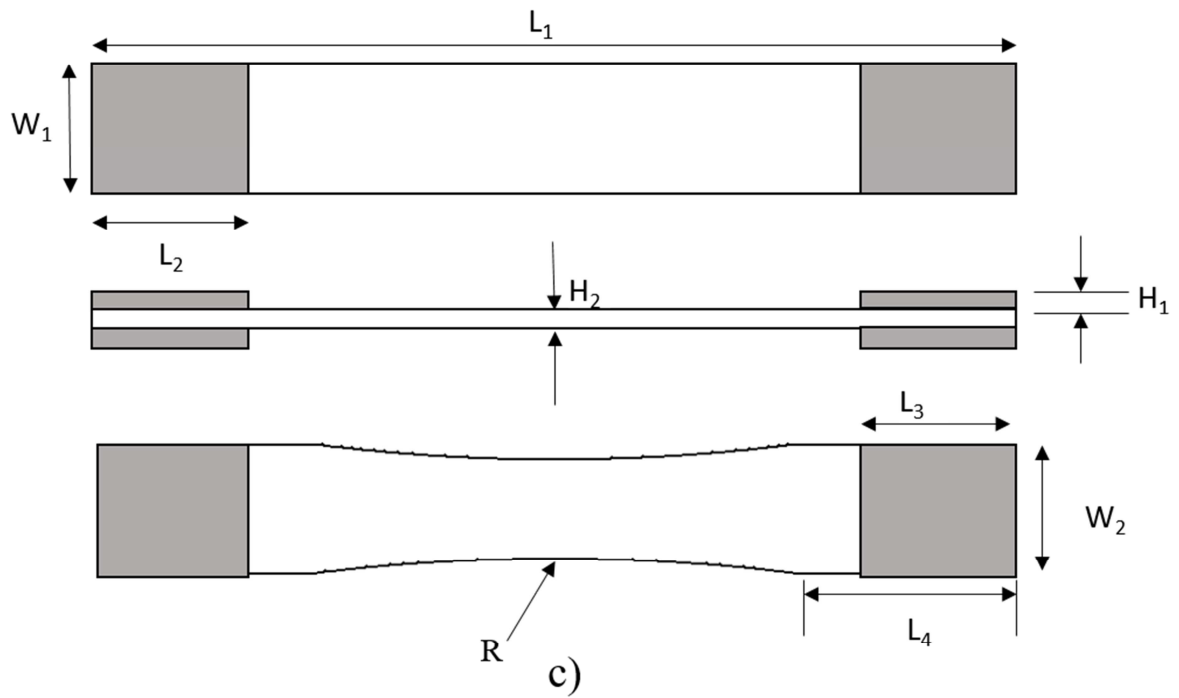
Laminations	L_3 (mm)	L_4 (mm)	W_2 (mm)	R(mm)	H_1 (mm)	H_2 (mm)
$[0_2/90_2]_s$	20	25	20	165	10	1.4 ± 0.1
$[0_4/90_4]_s$	20	25	20	165	10	2.8 ± 0.1



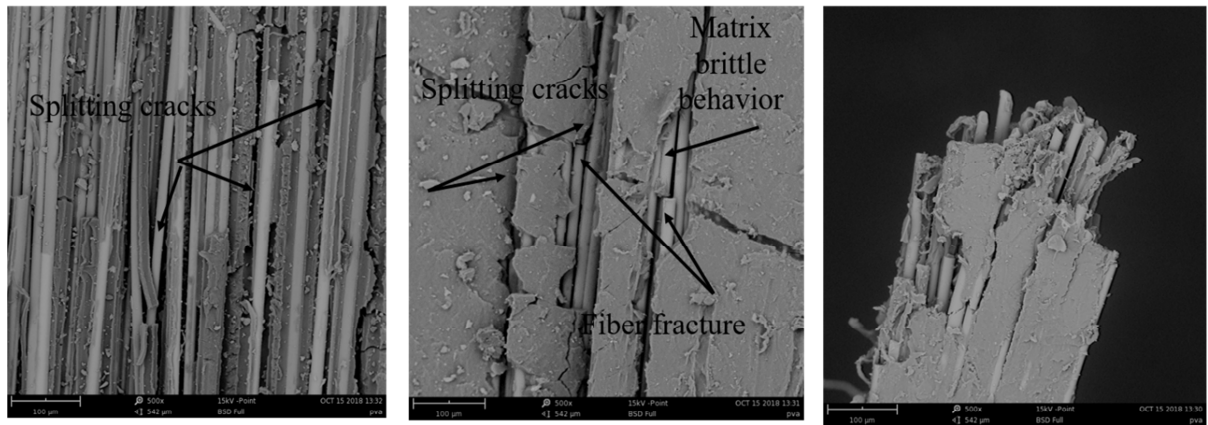
a)



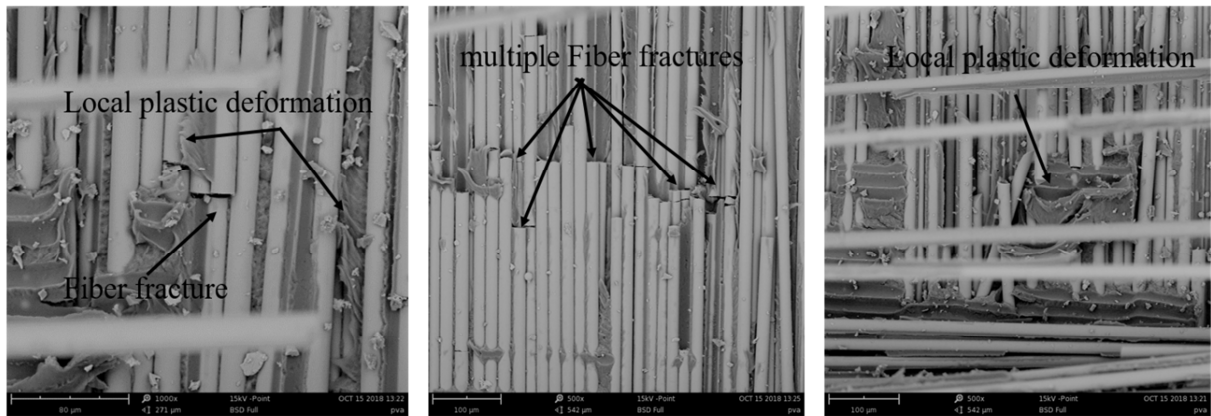
b)



c)

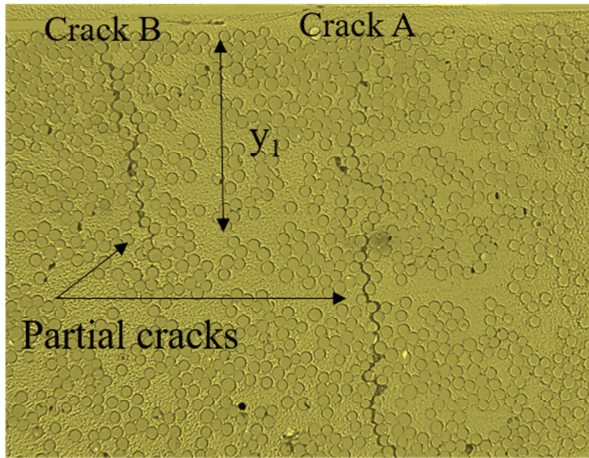


a)

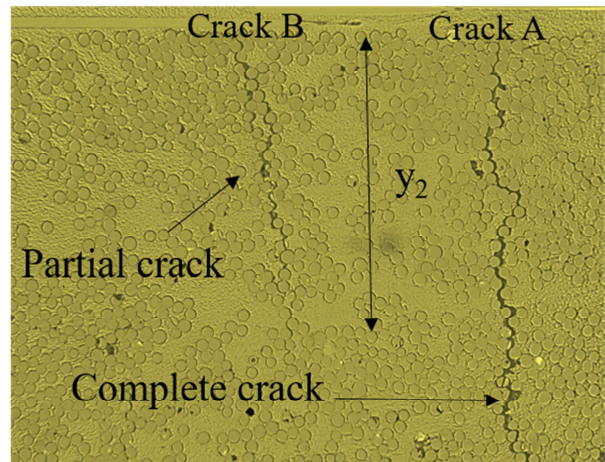


b)

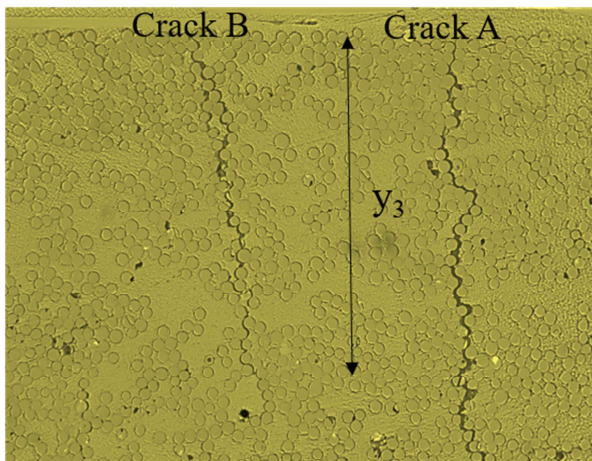
ACCEPTED



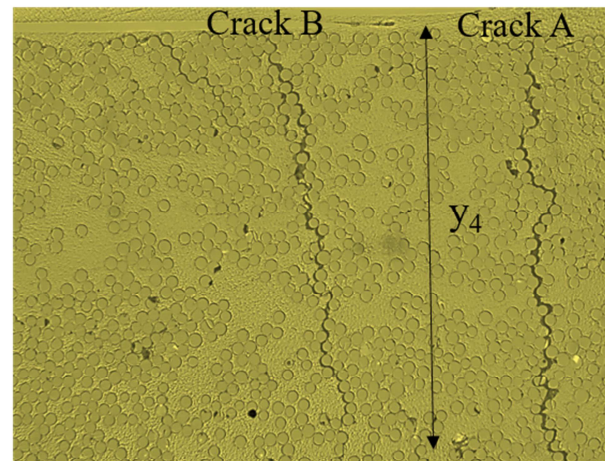
N=50



N=350

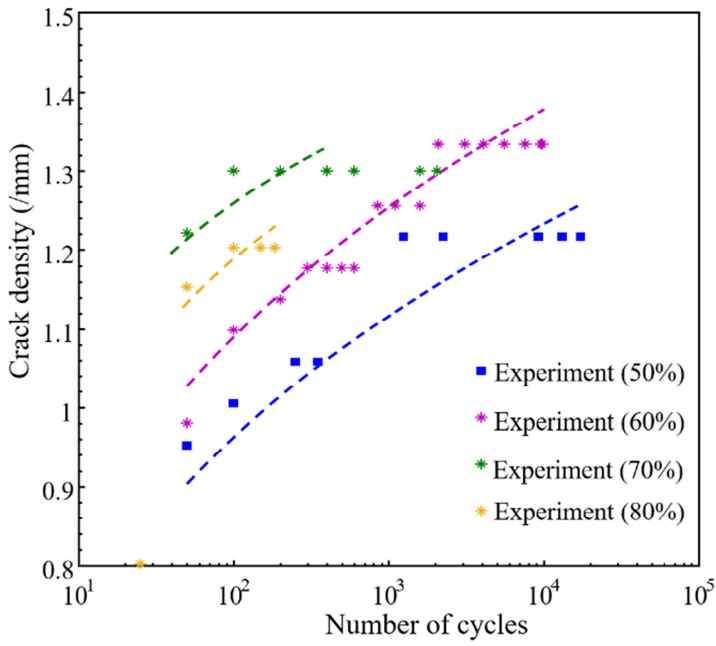


N=1250

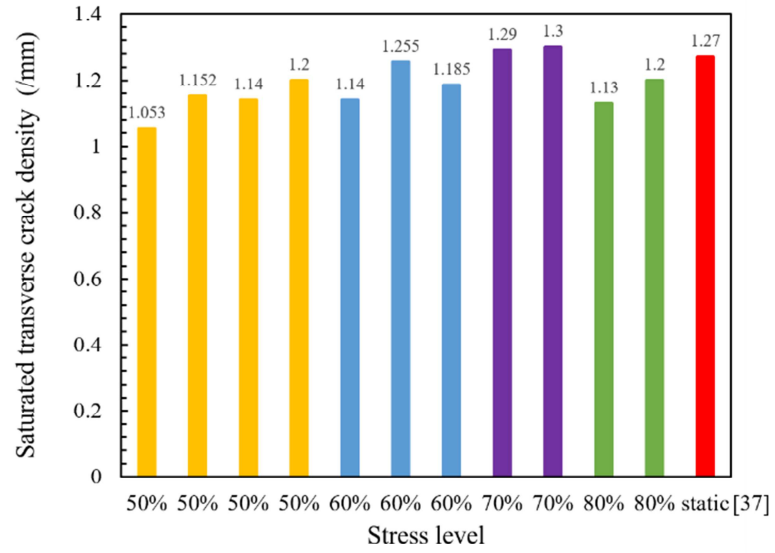


N=13250

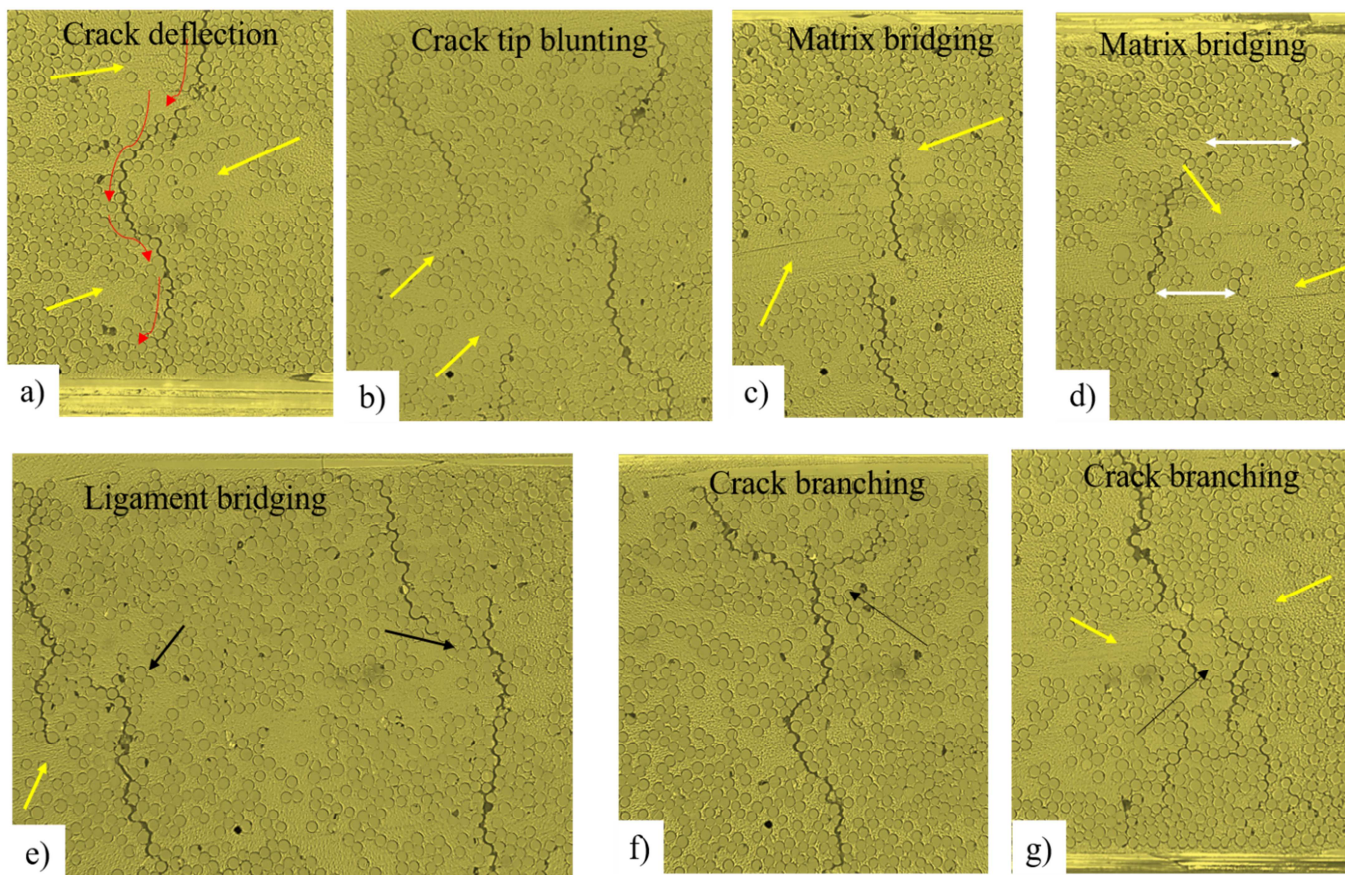
ACCEPTED



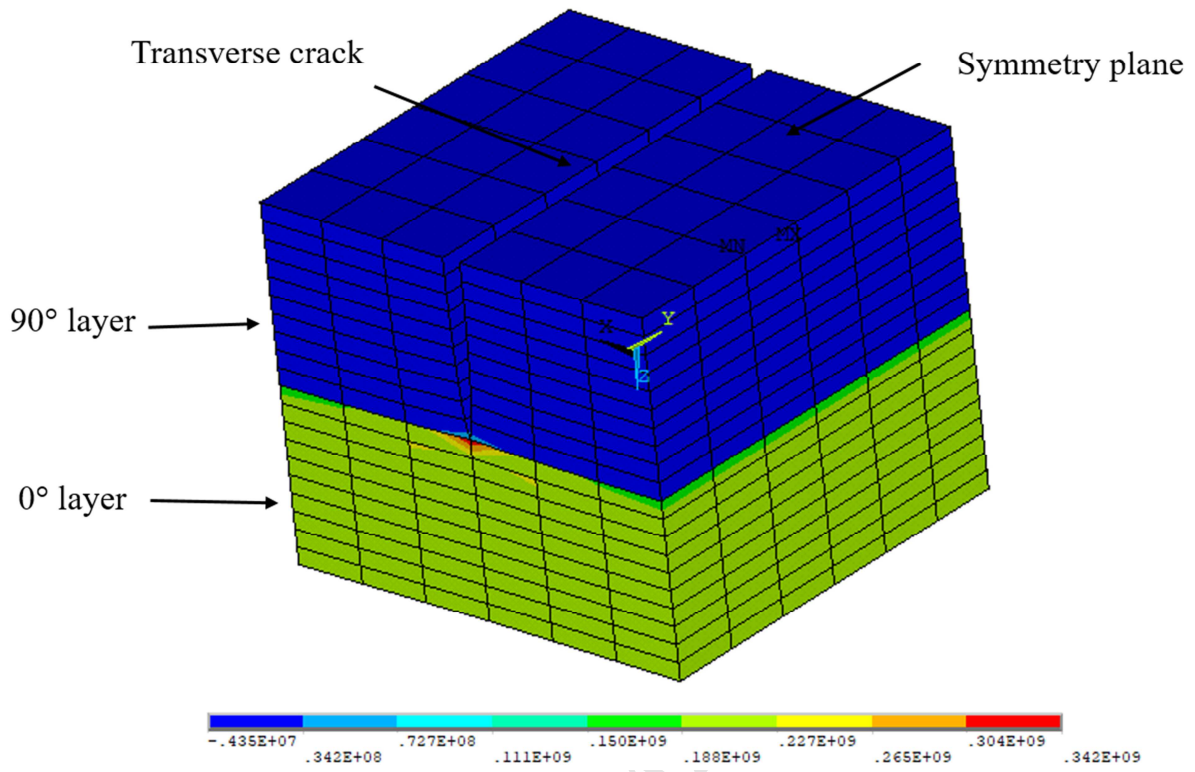
a)

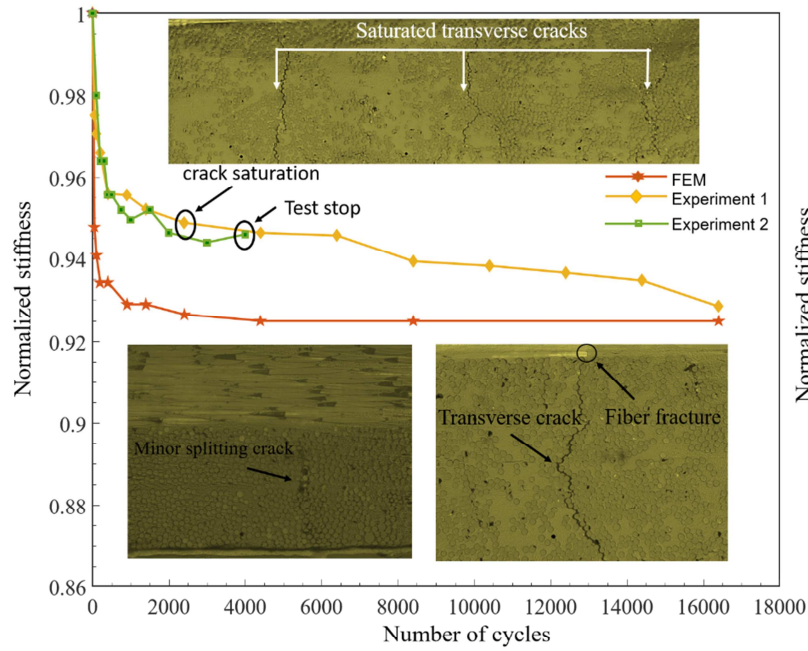


b)

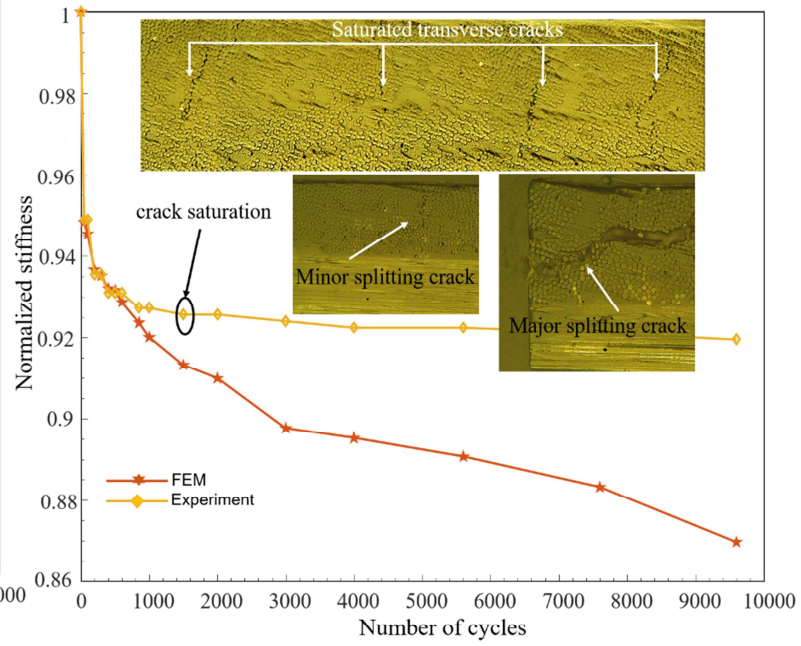


ACCEPTED

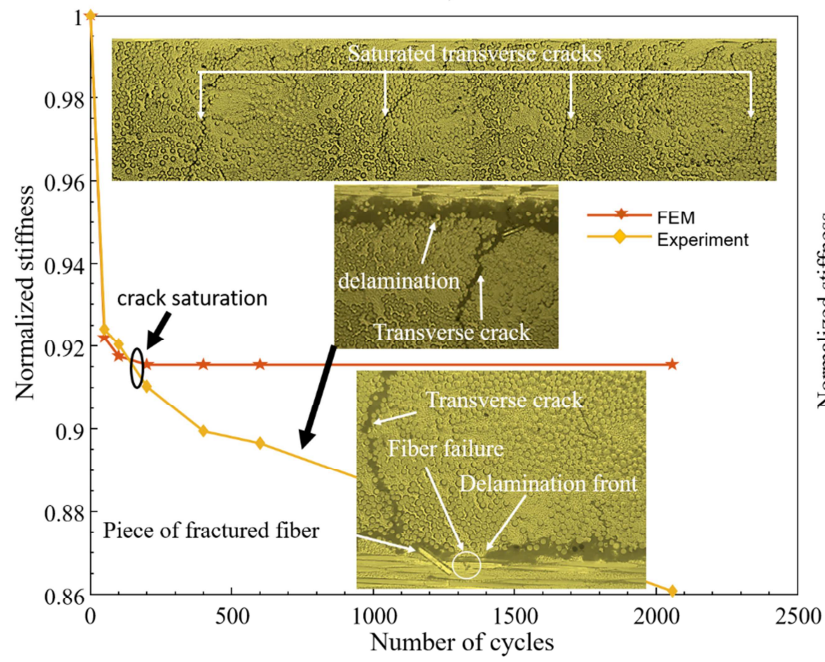




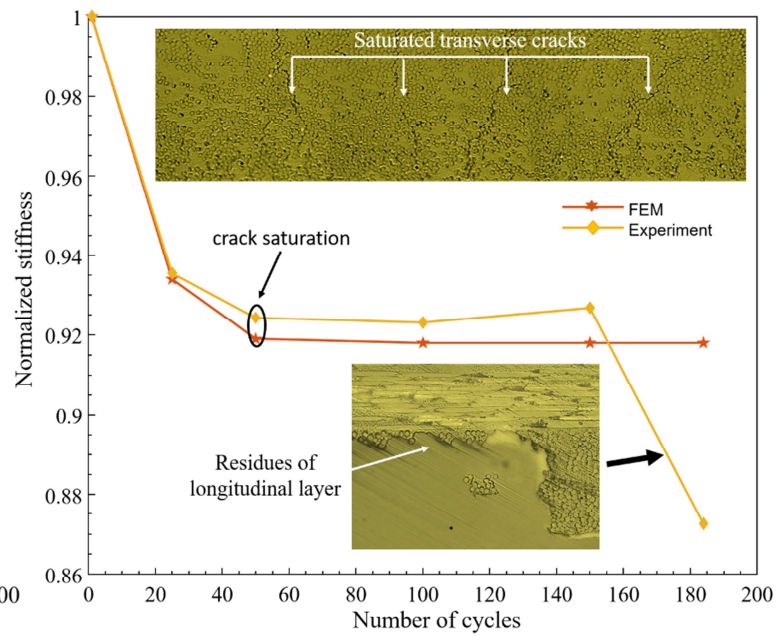
a)



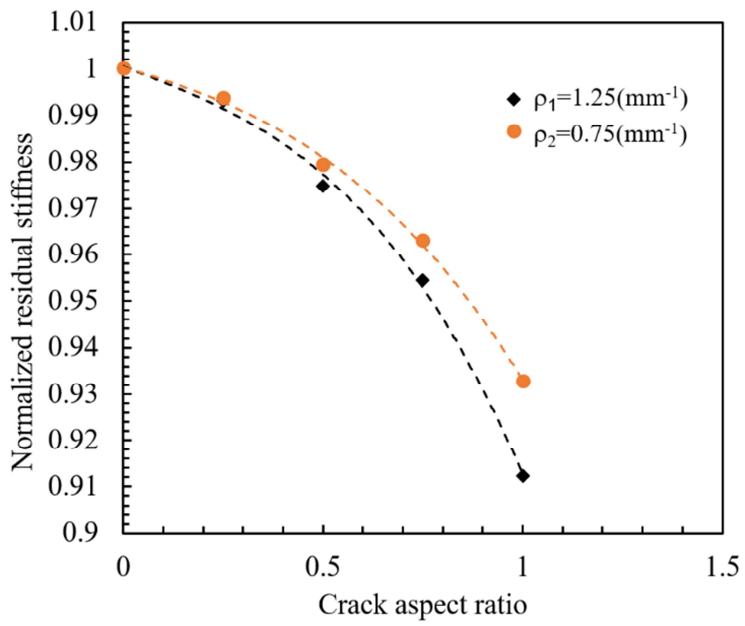
b)



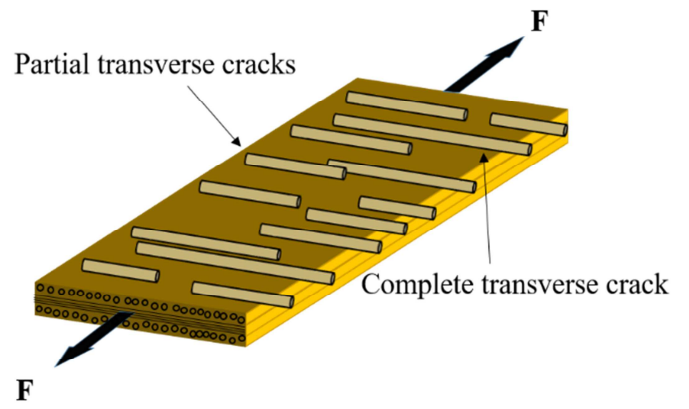
c)



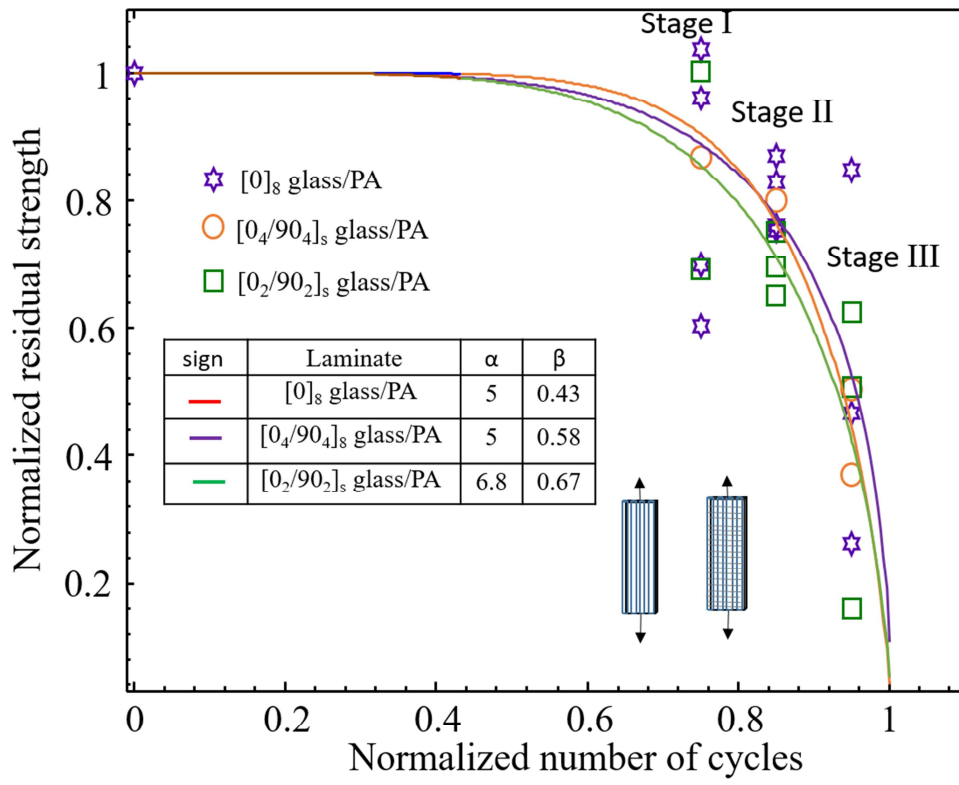
d)

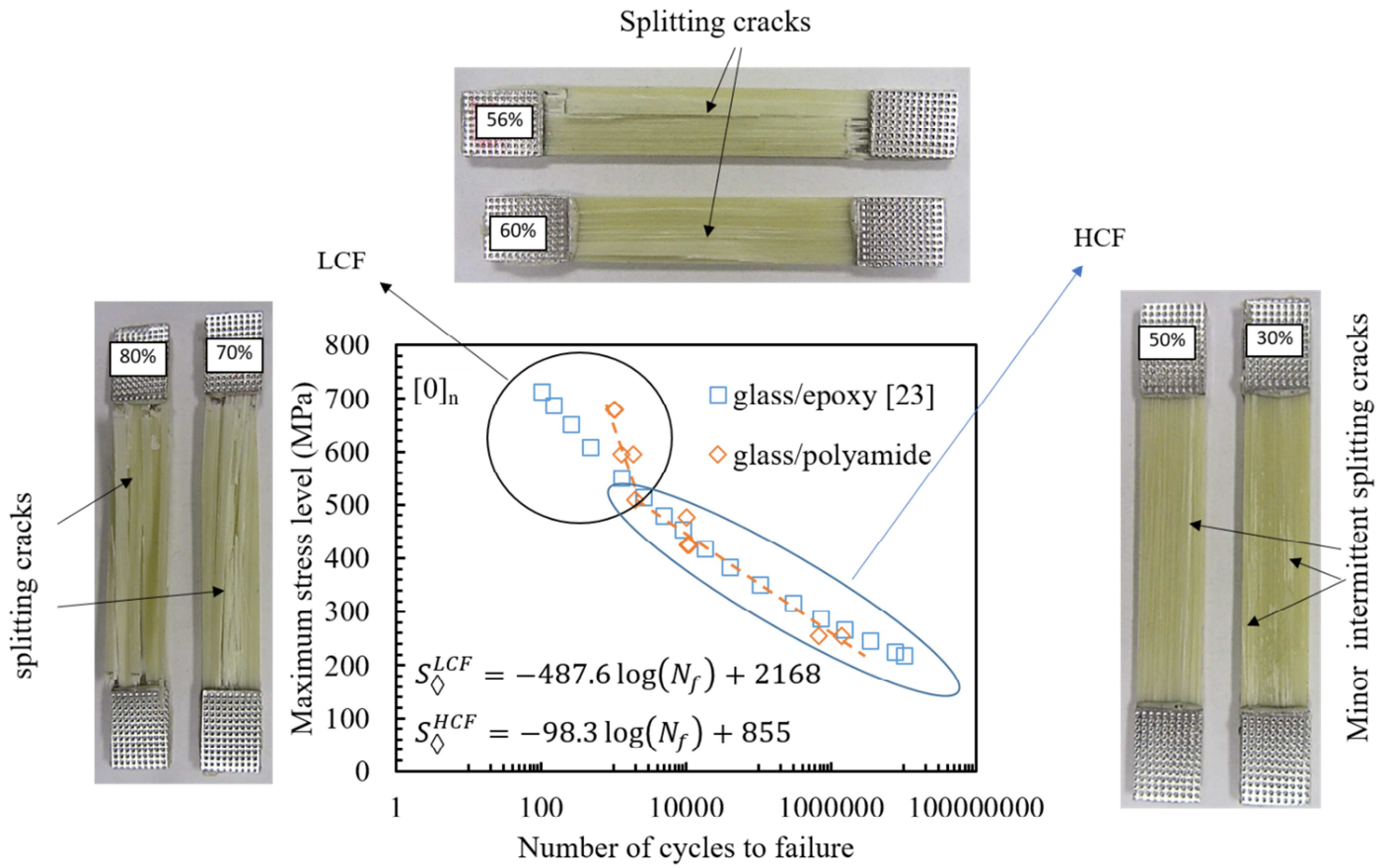


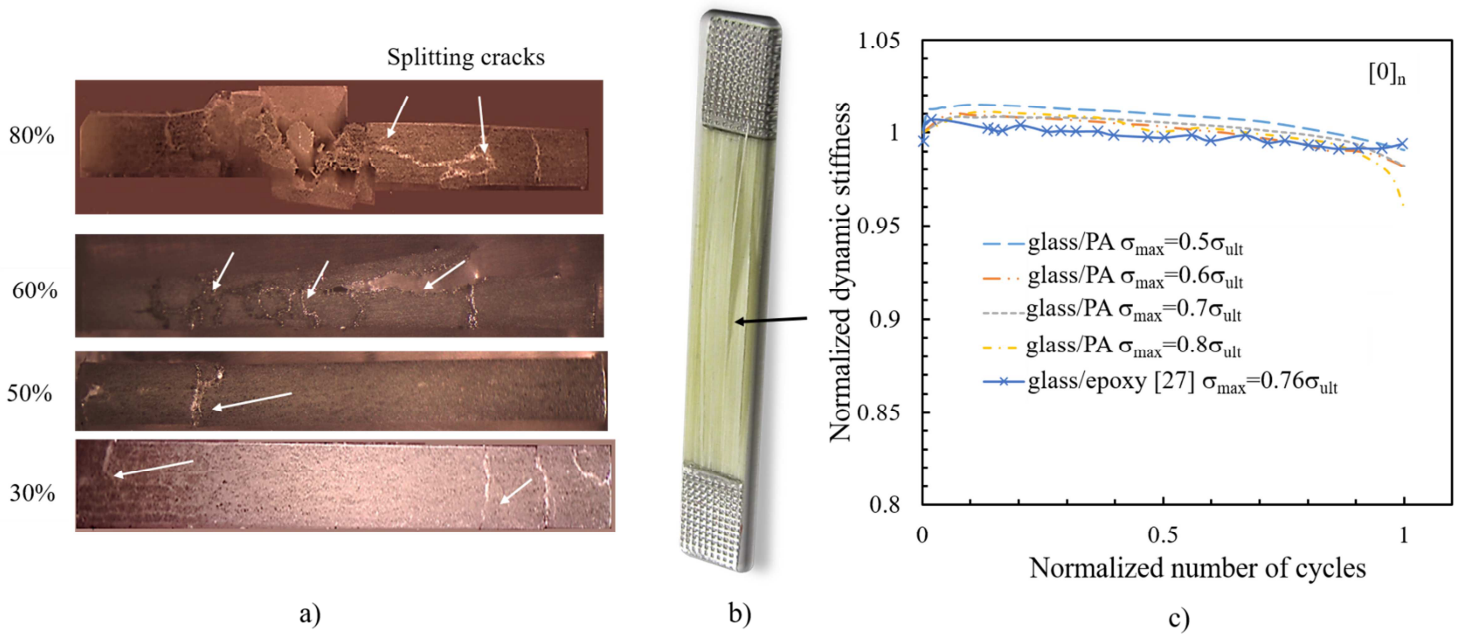
a)

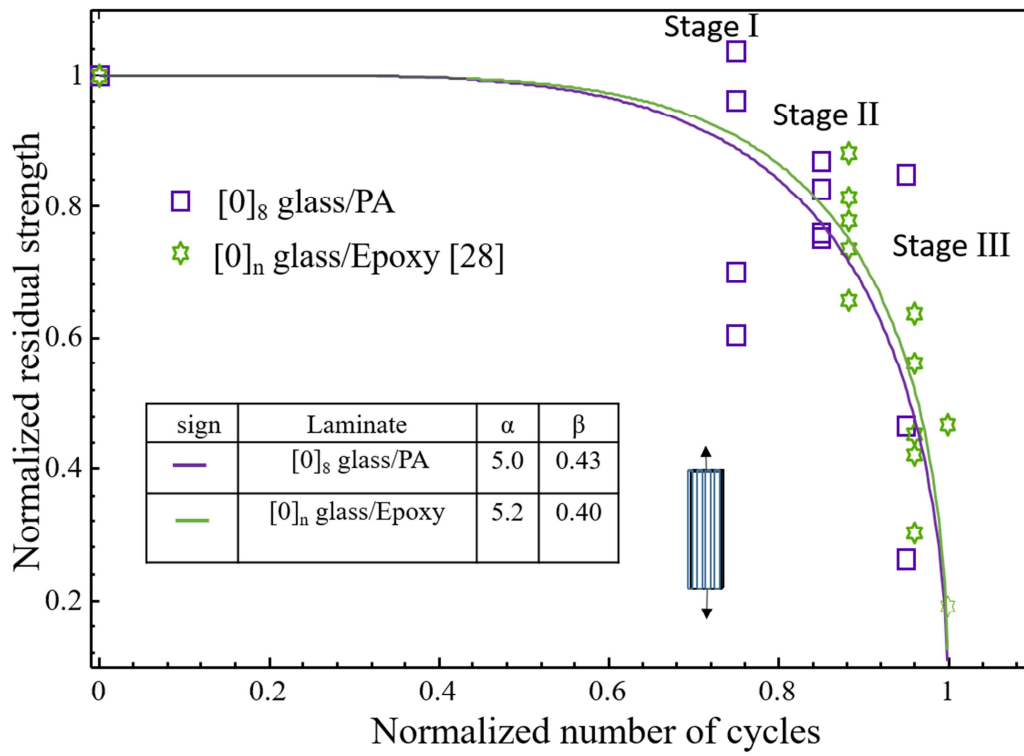


b)

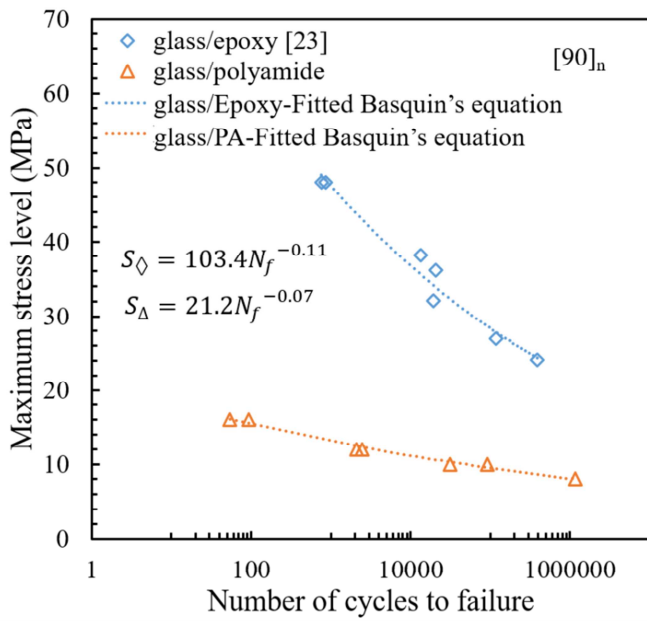




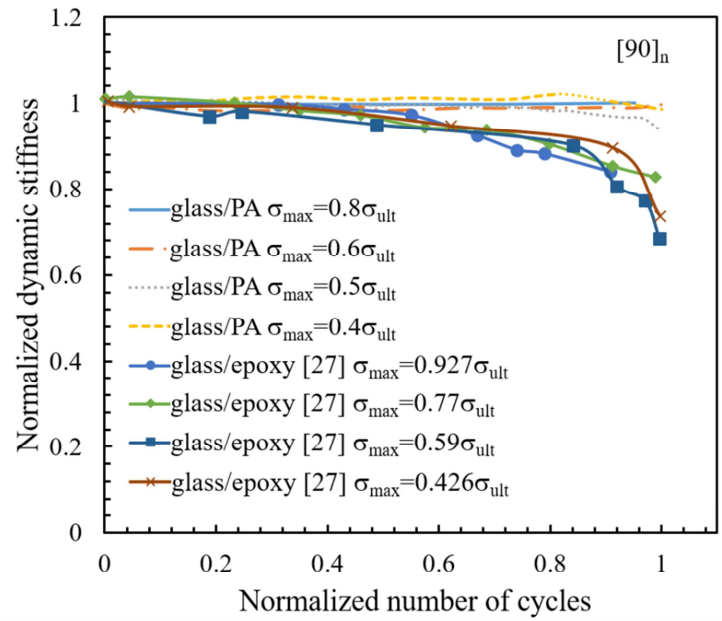




ACCEPTED MANUSCRIPT

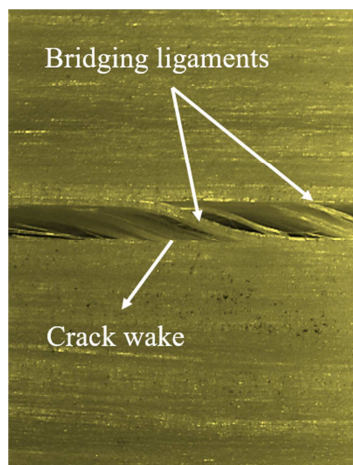


a)

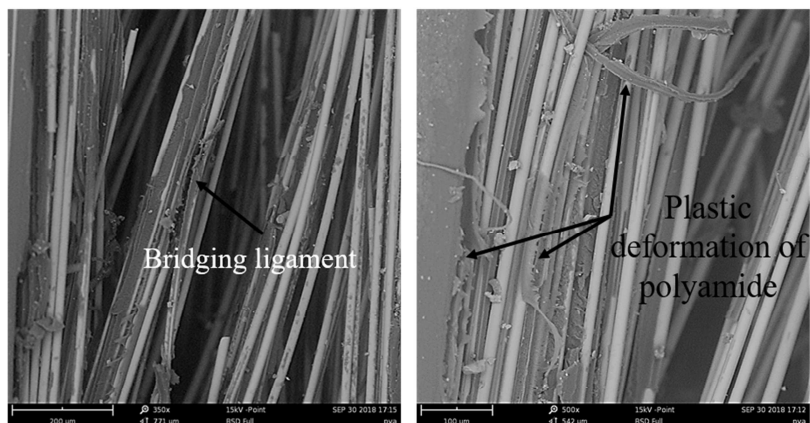


b)

ACCEPTED MANUSCRIPT

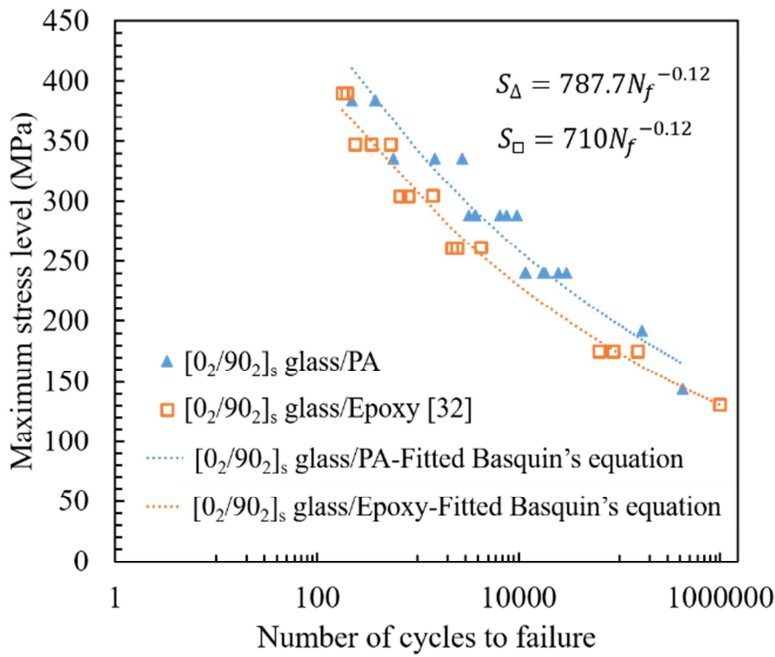


a)

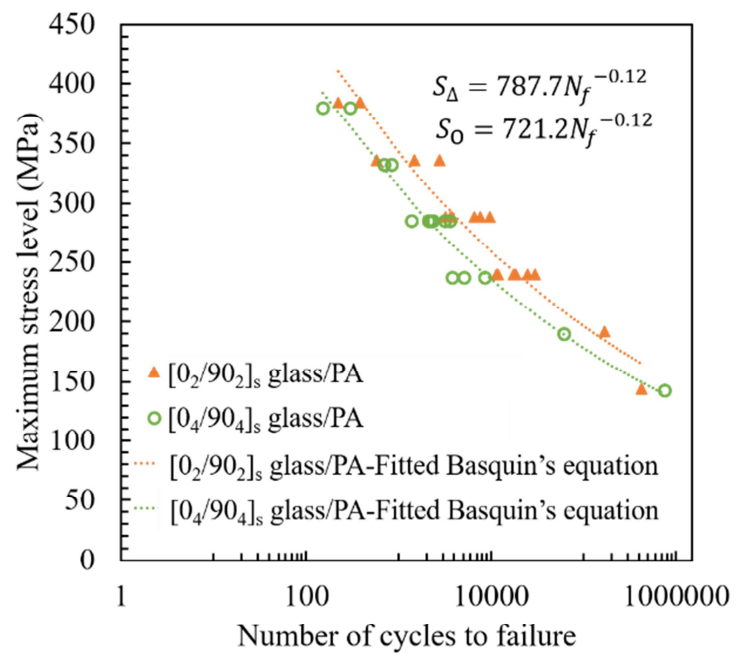


b)

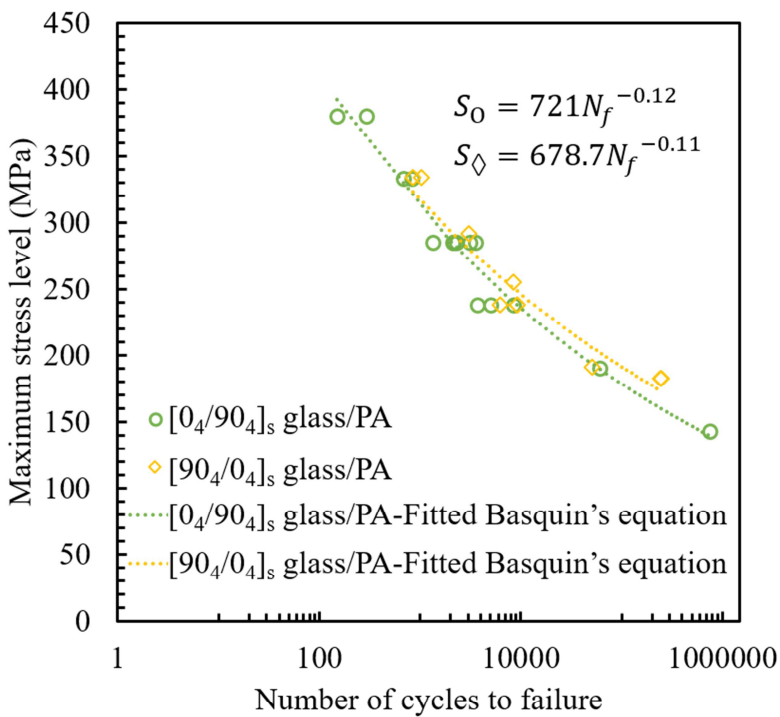
ACCEPTED MANUSCRIPT



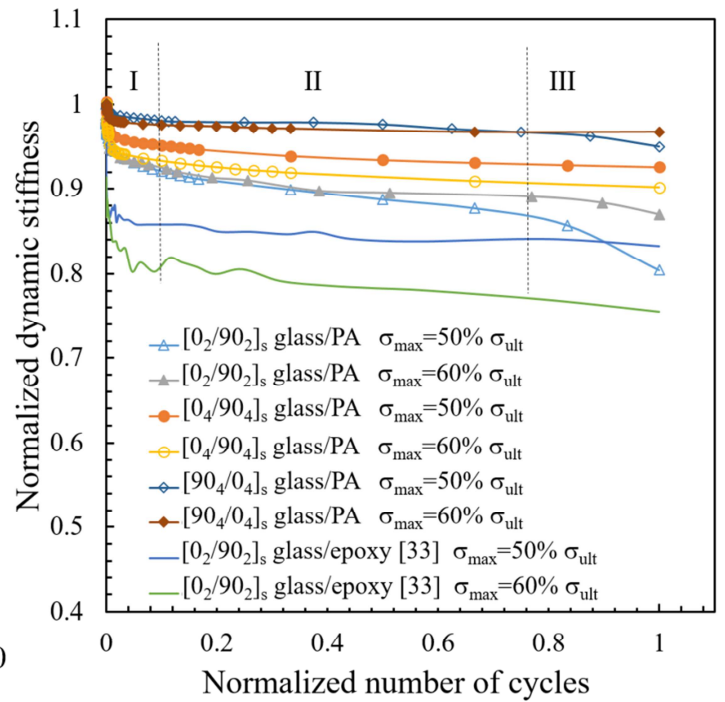
a)



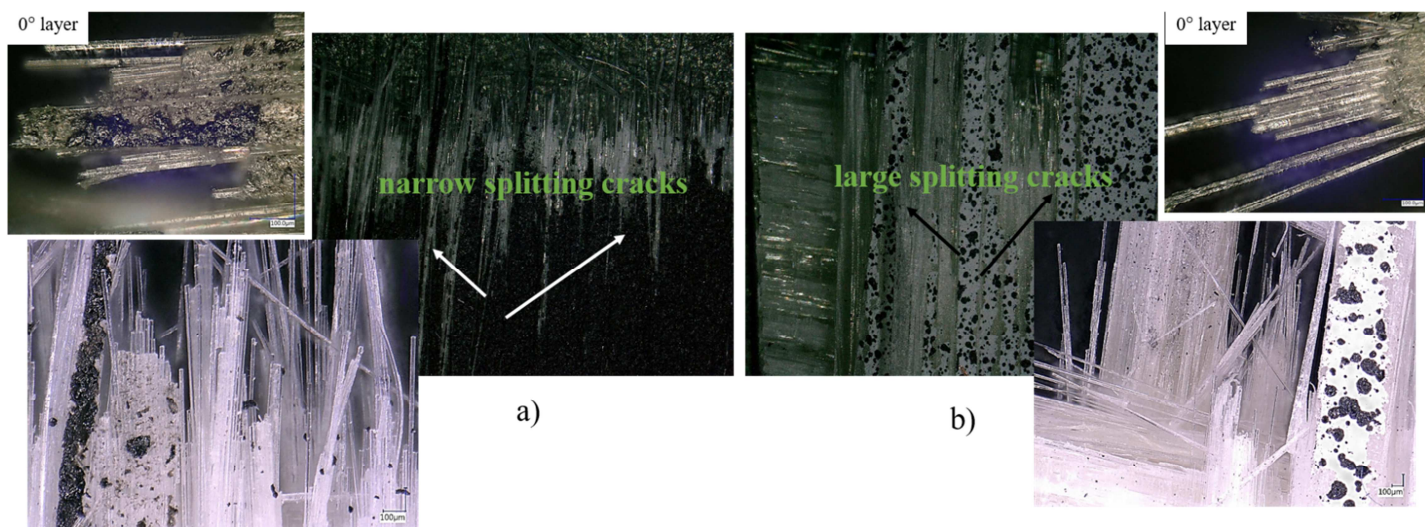
b)



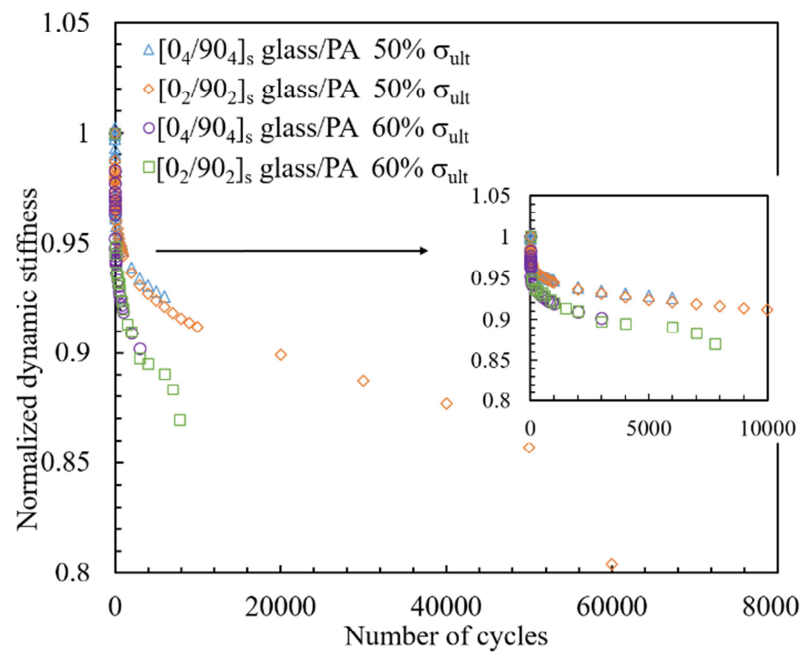
c)



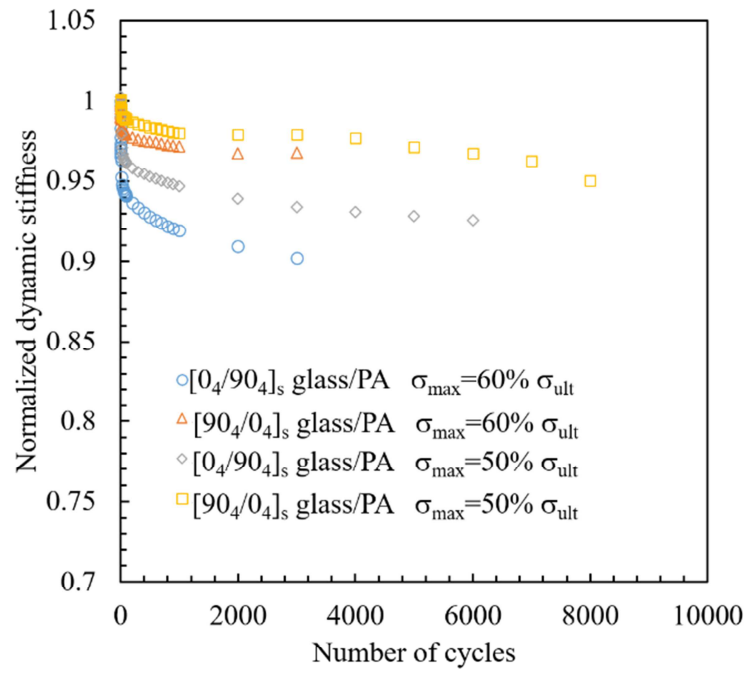
d)



ACCEPTED MANUSCRIPT



a)



b)

ACCEPTED MANUSCRIPT